Journal of
Marine Science and Engineering

MDPI

Article

Bearing Characteristics of Helical Pile Foundations for Offshore Wind Turbines in Sandy Soil

Yifeng Lin [1], Jiandong Xiao [1,*], Conghuan Le [2,*], Puyang Zhang [2,3], Qingshan Chen [2] and Hongyan Ding [2,3]

1 Shanghai Investigation, Design & Research Institute Co., Ltd., Shanghai 200355, China; lyf@sidri.com
2 School of Civil Engineering, Tianjin University, Tianjin 300072, China; zpy_td@163.com (P.Z.); zpy3000@21cn.com (Q.C.); dhy_td@163.com (H.D.)
3 State Key Laboratory of Hydraulic Engineering Simulation and Safety, Tianjin University, Tianjin 300072, China
* Correspondence: xjd@sidri.com (J.X.); leconghuan@163.com (C.L.)

Abstract: Helical pile foundations are a new foundation type for offshore wind power applications with high bearing capacity and good recovery that can be quickly and easily constructed. In this study, the finite element method was used to simulate the bearing characteristics of helical pile foundations after installation. For simulations, a blade, deeply buried in a single layer of sand, was selected. Through numerical simulations, the vertical bearing characteristics of a single helical screw pile and an ordinary pile without blades were compared, and the compression and uplift characteristics of the helical pile were revealed. In addition, the effects of pitch, blade diameter, inclination angle, number of blades, and blade spacing on the bearing characteristics of a single helical pile were analyzed. The results show that the single helical pile has the highest bearing capacity and bearing efficiency when the pitch is 0.02 times the blade buried depth, the blade diameter is 2.5 times the pile diameter, the multi-blade spacing is more than two times the blade diameter, and the number of blades is less than or equal to three. However, compared with the straight pile, the vertical bearing capacity of the single inclined helical pile did not improve significantly.

Keywords: helical pile; bearing capacity; numerical simulation

check for updates

Citation: Lin, Y.; Xiao, J.; Le, C.; Zhang, P.; Chen, Q.; Ding, H. Bearing Characteristics of Helical Pile Foundations for Offshore Wind Turbines in Sandy Soil. *J. Mar. Sci. Eng.* **2022**, *10*, 889. https://doi.org/10.3390/jmse10070889

Academic Editor: Constantine Michailides

Received: 23 May 2022
Accepted: 23 June 2022
Published: 28 June 2022

1. Introduction

Helical pile foundations have been successfully used for large civil engineering structures since the nineteenth century. Steel pipe piles with blades are generally buried into the foundation by applying torque. Due to the additional bearing capacity provided by the blades, early applications of helical pile foundations were often in soft soil areas such as beaches [1], for example, the Maplin Sands Lighthouse. Helical pile foundations can solve the problem of insufficient bearing capacity of traditional pile foundations, and they were later used as foundations for offshore bridges [2].

With increasing installed capacity and the development of wind farms, from offshore to deep sea, offshore wind foundations present additional challenges [3–8]. The jacket foundation is suitable for sea areas with water depths greater than 30 m. The bottom of the jacket is usually a multi-pile foundation, which forms a drawing system to resist the large bending moment loads of offshore wind turbines [9]. In areas with soft foundations, the length of traditional pile foundations must be considerable to provide sufficient bearing capacity, resulting in huge costs. Moreover, pile sliding often occurs during the construction process, posing a potential safety hazard [10,11]. The helical pile foundation not only reduces pile sliding, but also provides a high enough bearing capacity and good economic performance due to the lower quantity of steel required.

As the most common form of foundation in offshore wind power, monopile foundations have been well studied worldwide for ultimate bearing capacity, long-term loading, and response under seismic loading [12–16]. Since the first application of the helical pile foundation, its bearing characteristics have been a major focus of research, particularly its vertical bearing capacity. For research purposes, early studies regarded the single-blade helical pile as a circular plate anchor, and failure modes in sandy soil were divided into shallow buried, transitional, and deep buried failure types. The shape of the sliding surface can be determined by the depth of the anchor plate and the relative density of the soil. As the shallow sliding surface penetrates the surface of the sand body, the failure modes can be further divided into cylindrical, inclined, and curved failure modes [17–22]. Two methods are commonly used to calculate bearing capacity: (a) Cylindrical shear method, which assumes that soil between the blades moves with the pile and the axial bearing capacity can be divided into three parts, including side friction of the upper pile, the friction of the outer soil between the blades, and end resistance formed by the uppermost blade or lowermost blade; (b) Independent bearing method, which calculates the reaction force of the pile body and each blade, then determines the total vertical bearing capacity by summation [23].

Some scholars have estimated the vertical bearing capacity of the helical pile based on the amount of torque generated during installation by assuming bearing capacity is positively correlated with torque [24,25]. Through finite element simulations of a helical pile in clay, Polishchuk et al. [26] showed that the bearing capacity of a double blade is 30% higher compared with a single blade. Interestingly, scholars have shown that simply increasing the size of the blade is not the most reasonable way to increase the bearing capacity of the spiral pile. Based on model tests of helical pile foundations in a soft clay layer overlying a sandy soil layer, Hassan [27] concluded that the spacing between blades is the main factor affecting the bearing capacity of double-blade helical piles, whereas increasing the blade size has no obvious effect on bearing capacity.

Relatively few studies have been performed on horizontal bearing capacity helical pile foundations. Prasad [28] directly compared the horizontal bearing capacity of an ordinary pile and helical pile using the rigid model pile test in cohesive soil. The blade increased the horizontal bearing capacity of the pile by 1.2–1.5 times. Ding [29,30] studied the cyclic installation torque and bearing capacity of a single-blade helical pile foundation in sand through model tests, considering the influence of both helical blade size and vertical force during installation. Other scholars have considered the influence of axial load on the horizontal bearing capacity of helical piles while ignoring soil disturbances due to installation. The lateral bearing capacity of the pile was found to increase under axial compressive loads and decrease under axial tensile loads [31].

Although research on the bearing capacity of helical piles has progressed considerably, there is still a lack of systematic analysis, especially in the offshore wind turbine environment. Furthermore, research on helical piles under the action of large bending moments or the inclined pile situation that may appear in pile group foundations is limited. In this paper, the influence of pitch and diameter of a single spiral blade, diameter and number of blades, and blade spacing of the helical pile on the compressive and tensile bearing capacity were comprehensively analyzed for the case of a helical pile in sand. The bearing characteristics of the helical pile and sensitivity of the blade arrangement were examined. In this paper, a large number of finite element analyses have been carried out on the influence of the helical blade arrangement on the bearing efficiency of helical pile foundations in saturated sandy soils, and the influence of the size and arrangement of helical pile foundations on bearing performance has been systematically studied, which can provide guidance for the design and optimization of helical pile foundations in practical engineering.

2. Numerical Model

2.1. Model Parameters

In this study, ABAQUS software package was used to analyze a three-dimensional finite element model of an offshore wind turbine helical pile foundation in sand. The vertical bearing characteristics of different types of helical piles under various working conditions were studied. Geotechnical media are highly complex, and their behaviors are dependent on several geotechnical factors such as structure, density, and pore water. The mechanical properties of geotechnical media can be simulated in ABAQUS, including the nonlinear stress–strain relationship, transient consolidation, stress-deformation behavior, stability of the rock and soil, and bearing capacity of the pile [32].

Taking the model presented in this paper as an example, the modeling process for the helical pile foundation can be divided into three parts, namely the helical pile, soil core inside the pile, and soil outside the pile. The C3D8R element was used to model the soil, and the S4R shell element was selected for the helical pile. The overall number of meshes in the model ranges between 80,000 and 120,000. During mesh generation, a denser mesh was used near the foundation in sand and the mesh in the periphery was sparser; the mesh representing connection between the pile body and the blade was dense, and it became sparser farther away; the inner and outer meshes of corresponding positions of the model should be as consistent as possible to ensure transmissibility and calculation accuracy, as shown in Figure 1.

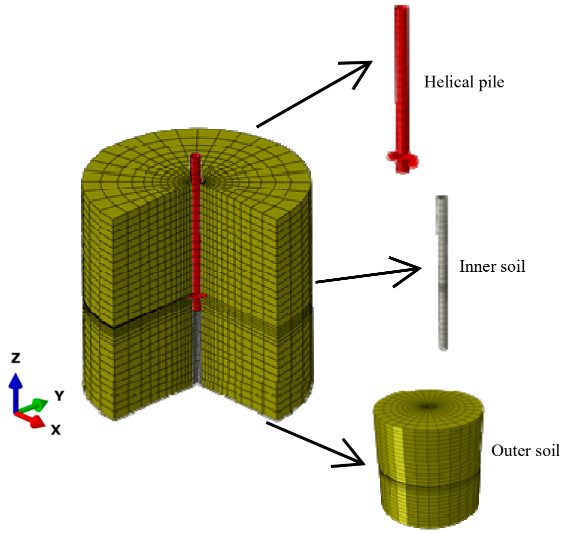

Figure 1. Mesh division for single helical pile model.

A schematic diagram of the helical pile foundation is shown in Figure 2, where d is the pile diameter, *D* is the blade diameter, *L* is the blade buried depth, *H* is the distance between the blade and the pile bottom, *l* is the blade spacing, *p* is the pitch, *T* is the pile thickness, and *t* is the blade thickness.

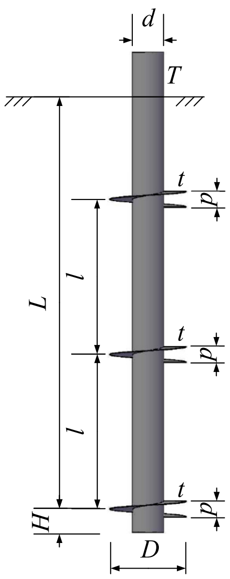

Figure 2. Schematic diagram of helical pile.

The stress–strain relationship of soil is complex. At present, no constitutive model can accurately and comprehensively express the constitutive relations of the various properties of soil under any loading mode. To analyze the bearing characteristics of helical pile foundations, the Mohr–Coulomb constitutive model is most appropriate and was selected in this study. In coastal areas, soil refers to sand. The soil parameters are listed in Table 1.

Table 1. Geotechnical properties of tested soil.

Items	Properties
Saturated density (g/cm^3)	2.2
Internal friction angle (°)	34.4
Cohesion (kPa)	5
Compression modulus (MPa)	18
Poisson's ratio	0.3

2.2. Boundary Conditions

The mechanical transfer characteristics of the contact surface between two types of media can be directly defined in ABAQUS. The mechanical model and contact constraint conditions of the contact surface force transfer can be established, and the contact constraint equation is then solved using the Lagrange multiplier method or penalty stiffness method [32]. To establish the pile–soil contact model, the surface of a spiral pile with a higher stiffness was selected as the main surface, and the soil surface in contact with the pile body and blade was selected as the secondary surface. The normal interaction between the two bodies is hard contact. Under compression, the normal stress between the surfaces can be modeled according to the contact constraint conditions between master and slave surfaces; under tensile stress, the contact surfaces are separated to produce a gap, contact constraints and friction between the contact surfaces do not exist, and there is no limit on the pressure transferred during contact.

Friction models are often used to simulate tangential mechanical behavior at an interface, and the penalty function method can simulate tangential interaction. A penalty stiffness function factor of elastic sliding was introduced to allow small elastic relative sliding at the bonded interface. Based on experience, the friction coefficient between the sand and the helical pile was set to 0.3.

The following boundary conditions were defined: a fully-fixed constraint (U1 = U2 = U3 = UR1 = UR2 = UR3 = 0) was adopted at the bottom of the soil, and displacement and rotation were not allowed in any direction; a radial constraint (U1 = U2 = UR3 = 0) was adopted on the side of the soil body and only displacement and torsion in the vertical direction were allowed; a free end was adopted at the upper part of the soil.

2.3. Loading Mode and Bearing Capacity Criterion

In this study, the displacement control method was selected. The displacement action point was coupled with the center pile top on the soil surface, and the load-displacement curve was obtained.

The ultimate bearing capacity of the pile foundation can be determined from the load-displacement curve. According to relevant specifications, the pile top angle of the offshore wind turbine foundation should be controlled within 0.005 radians, and the vertical settlement should be controlled within 100 mm. Thus, the load produced by a vertical displacement of 0.1 m was selected as the vertical ultimate bearing capacity of the single pile.

2.4. Numerical Model Verification

The finite element model was verified by test results using a large-scale model of a single-blade screw pile carried out by Wang [33]. The same soil and pile dimensions were used in simulations, and the load and displacement were normalized. The soil is dense sand, the pile depth-to-diameter ratio L/D is 5, and the dimensionless uplift bearing coefficient can be calculated as:

$$N_0 = \frac{V}{\gamma' LA} \tag{1}$$

where N_0 is the dimensionless uplift bearing coefficient, V is the uplift load, γ' is the effective bulk density of the soil, and A is the single side area of the helical blade.

A comparison of the simulation results and experimental data is presented in Figure 3. The experimental data fluctuates; however, overall, there is little difference between the curves obtained by numerical simulation and experiment, indicating that the numerical results are reasonable and representative of the bearing characteristics of the spiral pile in sand.

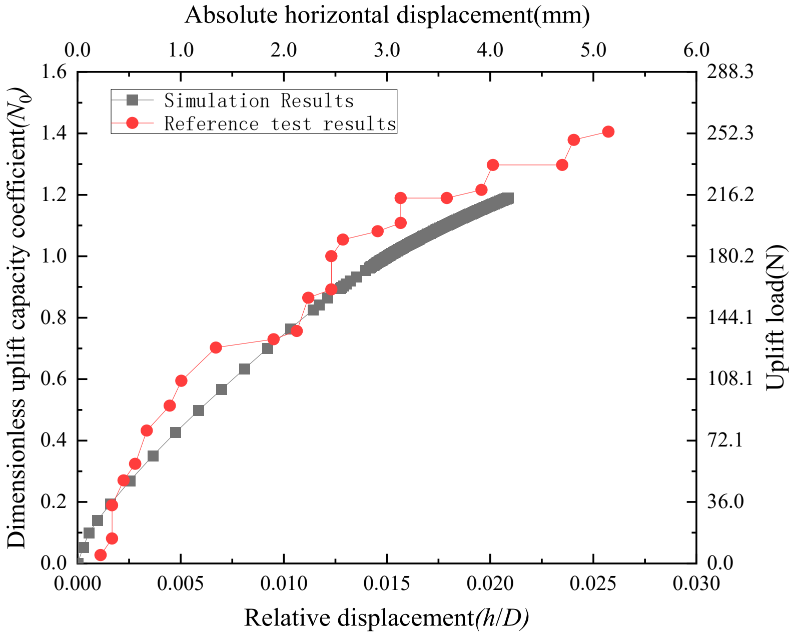

Figure 3. Comparison of finite element simulation results and experimental data of Wang et al. [25].

3. Study on Bearing Capacity of Single Helical Pile and Monopile

3.1. Calculation Conditions

The influence of the helical blade and range of soil displacement was studied by comparing the displacement of a helical pile and monopile in single-layer sand. The specific parameters and dimensions of the helical pile and monopile are presented in Table 2. The dimensions of the helical pile and the ordinary pile were the same, except for the blade.

Table 2. Dimensions of monopile and helical pile.

Items	Helical Pile	Monopile
Diameter (m)	2	2
Number of blades	1	0
Pile length (m)	25	25
Blade diameter (m)	5	-
Pitch (m)	1	-
Distance between blade and pile bottom (m)	1.5	-

3.2. Horizontal and Bending Moment Capacity

Load-displacement curves of the pile foundation were obtained by applying a displacement far greater than the expected bearing capacity at the top center of the foundation pile. Then, the load and displacement at failure were determined in order to determine the corresponding bearing capacity.

After applying an excessive horizontal displacement and rotation angle, load-displacement curves of the monopile and helical pile were obtained, as shown in Figure 4. The horizontal bearing capacity and bending moment bearing capacity of the helical pile and the monopile are almost the same because the spiral blade is deeply buried and therefore has little influence. The screw pile foundation has the same horizontal load pattern as the monopile foundation. Therefore, the rest of this paper will focus on the vertical bearing capacity and bearing modes.

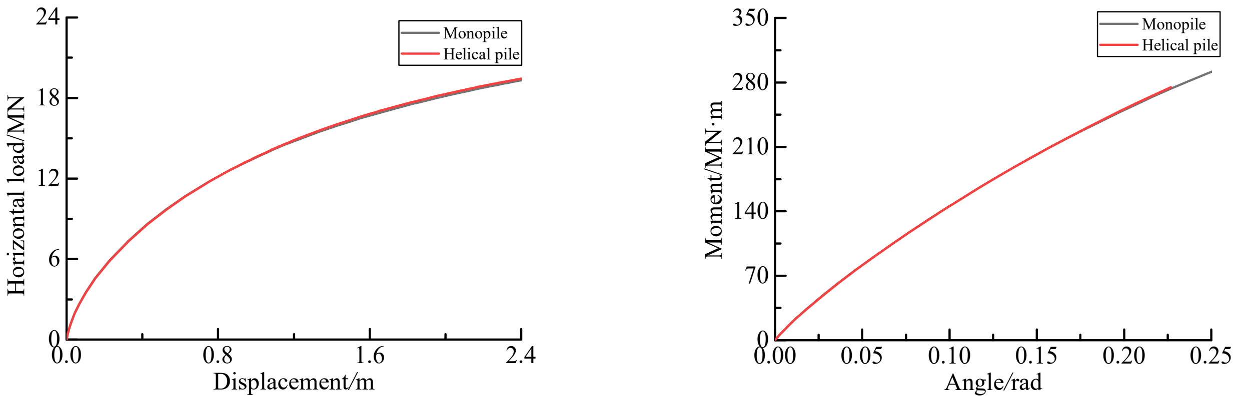

(**a**) (**b**)

Figure 4. Horizontal and moment capacity of helical pile and monopile. (**a**) Horizontal capacity; (**b**) Moment capacity.

3.3. Compressive Capacity

After applying excessive vertical downward displacement, compressive load-displacement curves of the monopile and helical pile were obtained, as shown in Figure 5. When the vertical displacement reaches 0.1 m, that is, 0.05 *D*, the compression bearing capacities of the monopile and helical pile foundations are 3.77 MN and 9.38 MN, respectively. The bearing capacity of the helical pile is 149% higher. When a compressive load is applied, both types of foundation first enter the elastic stage, and the curve grows linearly. In the plastic stage, the slope of the single pile curve is gentle, and the slope of the spiral pile is slightly lower. The helical blade results in a higher bearing capacity.

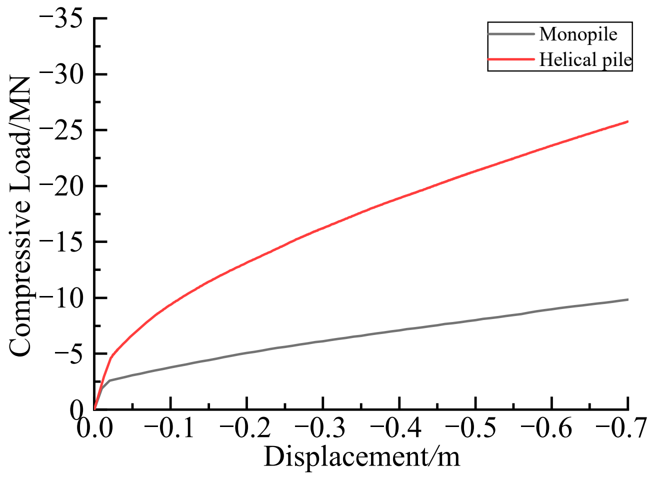

Figure 5. Compressive load-displacement curve.

The displacement nephogram of the soil around the pile for an applied compressive load of 7 MN is shown in Figure 6. The vertical displacement of the monopile foundation is 0.39 m, and that of the spiral pile is 0.055 m. The deformation of the helical pile is much smaller than that of the monopile. Displacements of the helical pile and monopile are largest at the bottom of the pile and develop into the surrounding soil. Due to the anchoring effect of the spiral blade, the soil around the pile bears more load and provides a certain bearing effect. The influence of displacement of the helical pile side soil is much larger compared with the monopile.

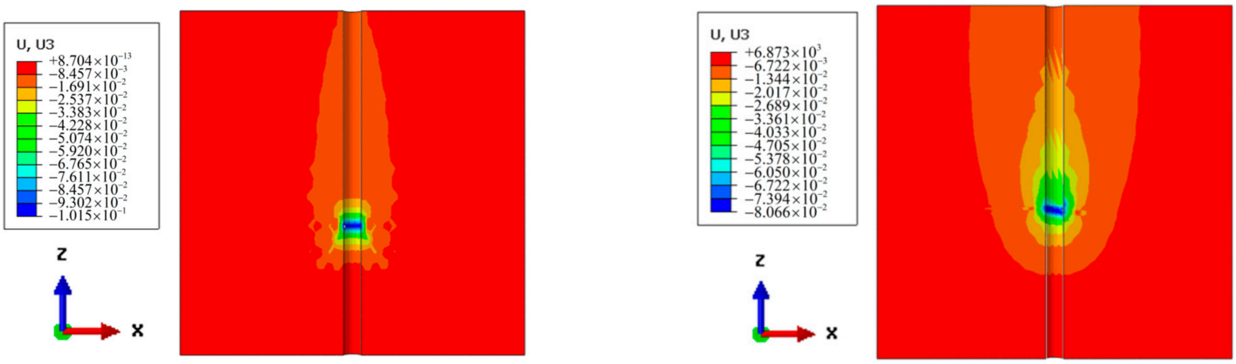

(**a**) (**b**)

Figure 6. Displacement nephogram of soil around the piles. (**a**) Monopile; (**b**) Helical pile.

As shown in Figure 7, vertical stress changes slightly at the pile end, and stress mutation occurs at the pile end, which is more obvious with the ordinary pile. Stress in the upper part of the pile tip is larger than that in the lower part. Compared with the monopile foundation, the area of concentrated stress in the helical pile foundation is smaller and the stress is higher.

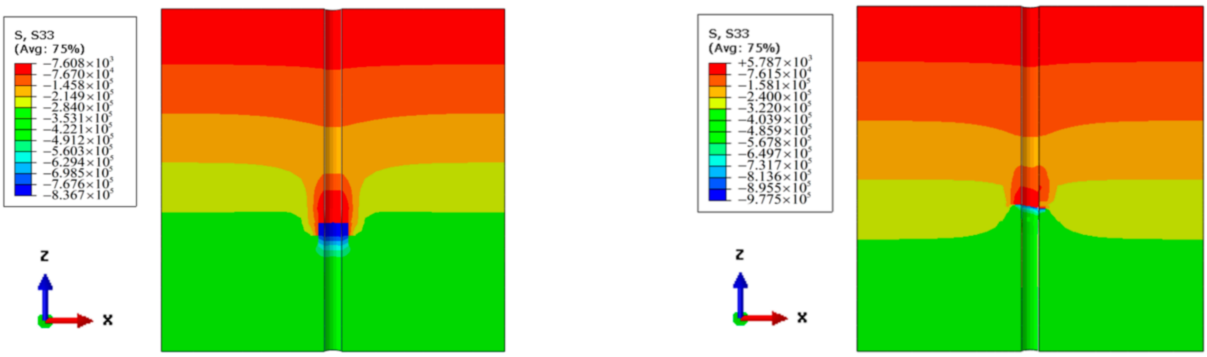

(**a**) (**b**)

Figure 7. Stress nephogram of soil around the piles. (**a**) Monopile; (**b**) Helical pile.

The variation of vertical stress in the soil on the side wall of the pile in the depth direction is shown in Figure 8. The change in stress of the monopile is relatively sharp, first increasing gradually with depth, then exhibiting a sharp increase or even mutation at about 25 m. The soil in the pile reached a maximum of 25 m. The maximum values were 0.54 MPa and 2.75 MPa, for the helical pile and the monopile, respectively, representing a five-fold difference. Locations of stress concentrations outside the pile are different. The stress of the soil surrounding the pile reaches a maximum at the lower part of the pile bottom, whereas the stress concentration of the helical pile is located at the blade. The maximum pressure of the monopile was 2.02 MPa, and that of the helical pile was 0.81 MPa. The blade greatly alleviates damage to the soil, thereby reducing the stress concentration.

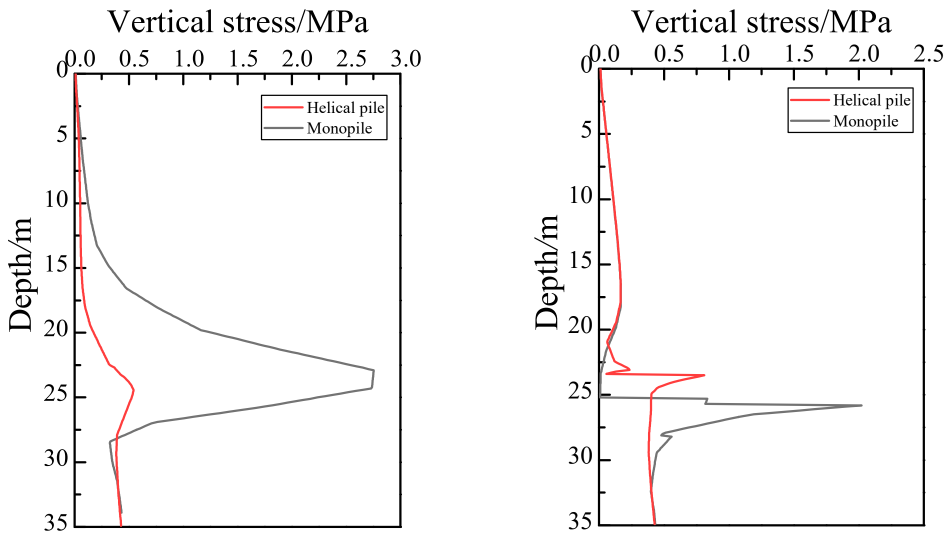

(**a**) (**b**)

Figure 8. Soil stress inside and outside the pile varies with depth. (**a**) Soil stress in pile; (**b**) Soil stress outside pile.

3.4. Tensile Capacity

According to Figure 9, the blade greatly increases the vertical bearing capacity of the pile. When the foundation bears an uplift load, the monopile reaches the ultimate bearing capacity before the vertical displacement reaches 0.06 m, and the load remains stable, with increasing displacement. Then, the helical pile still has a significant increase, and the uplift capacity is significantly improved.

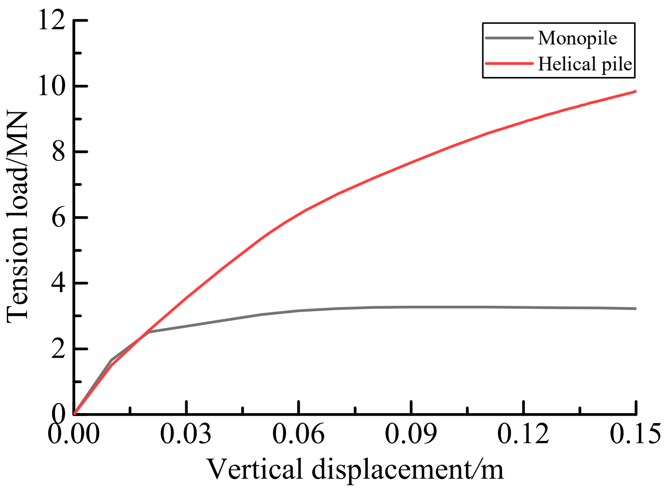

Figure 9. Uplift load-displacement curves.

Displacement nephograms of soil around the pile with an uplift displacement of 0.1 m are shown in Figure 10. When the pullout displacement reaches 0.1 m, the influence of soil displacement around the helical pile is much larger compared with the monopile. The helical blade drives soil around the pile upwards, while friction between the side wall and the end of the pile only drives a small portion of the soil displacement.

Uplift load-displacement curves of the monopile and the helical pile were obtained under excessive vertical upward displacement, as shown in Figure 11. When the pullout displacement is 0.1 m, the pullout bearing capacity of the monopile is 3.27 MN, and that of the helical pile is 8.13 MN.

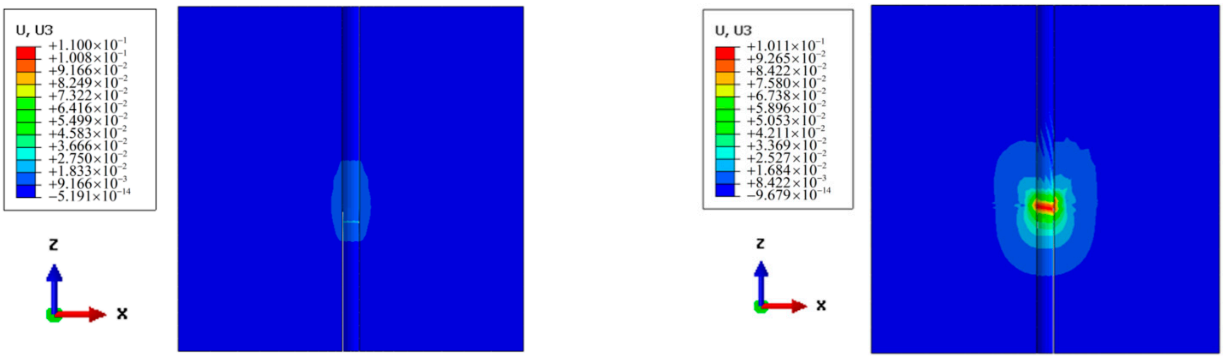

Figure 10. Displacement nephograms of soil around the piles. (**a**) Monopile; (**b**) Helical pile.

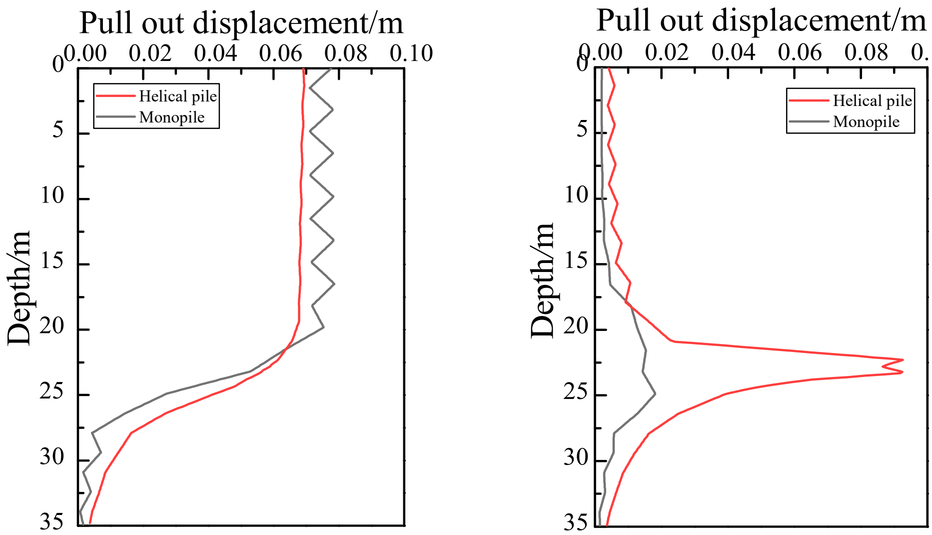

Figure 11. Soil stress inside and outside pile varies with depth. (**a**) Soil stress in pile; (**b**) Soil stress outside pile.

The pull-out displacement depth curves of the soil inside the two piles are similar, as shown in Figure 11. The displacement of soil within 20 m is about 0.07 m, and the displacement below 20 m decreases and gradually tends to 0. The displacement of soil outside the pile changes very little within 20 m, and the slope is gentle. The soil displacement increases around 20–25 m, then gradually tends to 0.

Compared with the monopile, the maximum displacement of soil outside the helical pile is 0.092 m, whereas that of the monopile is 0.018 m, representing a five-fold difference. Therefore, the blade results in more soil on the blade being pulled out, and the soil disturbance due to the helical pile is greater under the same displacement.

4. Effect of Pitch on Bearing Capacity of Single Helical Pile

4.1. Calculation Conditions

To study the influence of pitch, p, of the helical pile, p = 1 m, 2 m, 3 m, 4 m, and 5 m; that is, pitch/blade diameters, p/D, of 0.4, 0.8, 0.12, 0.16, and 0.2, were studied. The specific parameters used for each pitch condition are listed in Table 3. When an excess vertical displacement is applied at the coupling point of the pile top, the loading direction can be divided into upper and lower, and the compressive and uplift bearing capacities were calculated.

Table 3. Helical pile parameter for various pitch values.

Items	P1	P2	P3	P4	P5
Pile diameter (m)	2	2	2	2	2
Number of blades	1	1	1	1	1
Blade depth (m)	25	25	25	25	25
Blade diameter (m)	5	5	5	5	5
Pitch (m)	1	2	3	4	5
Distance between blade and pile bottom (m)	1.5	1.5	1.5	1.5	1.5

4.2. Compressive Capacity

The compressive load-displacement curves of helical piles with different pitches were obtained under excessive vertical downward displacement, as shown in Figure 12a. The load-displacement curves have an obvious elastic section and inflection point. Larger bearing capacities are obtained at the same displacement with P2, P3, and P4. When the indentation displacement is 0.1 m, P1 results in a compressive capacity of 9.39 MN, and P4 results in 9.93 MN, which represents an increase of 5.75%. Therefore, selecting the appropriate pitch can improve the compressive bearing capacity of the helical pile.

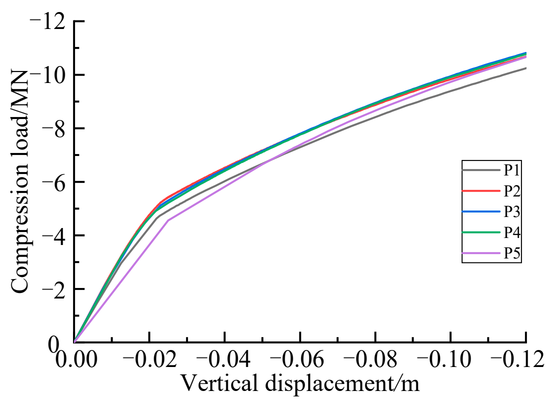

(**a**)

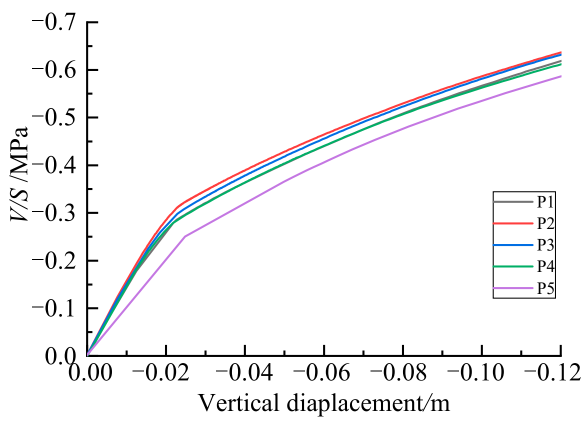

(**b**)

Figure 12. Compression bearing characteristic curves of helical pile with various pitches. (**a**) Load-displacement curves; (**b**) Vertical force/blade area (V/S)-displacement curves.

Increasing the pitch inevitably increases the blade area; therefore, the quantity of steel required increases. To eliminate this effect, the ratio of load to area was studied, as shown in Figure 12b. The abscissa represents vertical displacement, V, the positive direction represents pull-out, and the negative direction represents push-in. The ordinate represents the ratio of vertical force, V, to blade area, S, the positive direction represents tension, and the negative direction represents pressure. Variations of the V/S-displacement curves of the helical pile with pitch are similar. When the displacement of the pile top is 0.1 m, the V/S of each pitch helical pile is about 0.4–0.5 MPa. In terms of bearing capacity, P2 and P3 were better than other conditions, especially P2, which led to a higher bearing capacity. That is, when the pitch is 2 m, the bearing capacity of the helical pile is better, and the helical pile structure is more economical.

As shown in Figure 13, the range of displacement varies with helical pitch. The displacement range of the pile is greatly extended in the longitudinal direction when the helical pitch is large; however, there is little difference in the horizontal direction. The displacement nephograms for P1 and P5 are similar, and the displacement contour of soil outside the pile radiates along the vertical direction of the pitch. The larger the pitch, the more inclined the displacement contour and the larger the range of influence in the longitudinal direction.

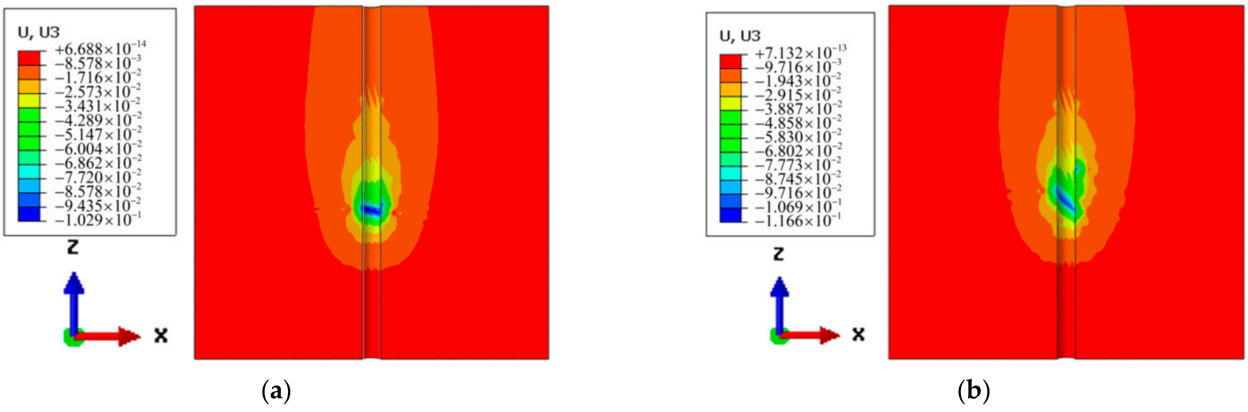

Figure 13. Displacement nephograms of soil around a pile with displacement of 0.1 m. (**a**) P1; (**b**) P5.

The von Mises stress nephograms of both pile types are shown in Figure 14. There is a sudden change in stress at the position of the helical blade, resulting in a stress concentration. The stress distribution is layered; however, small uplifts can be observed on the upper and lower sides of the spiral blade. The lower soil of the blade is subjected to a large compressive load, while the upper soil is suspended and settled; therefore, the stress is very small in the upper soil and very large in the lower soil.

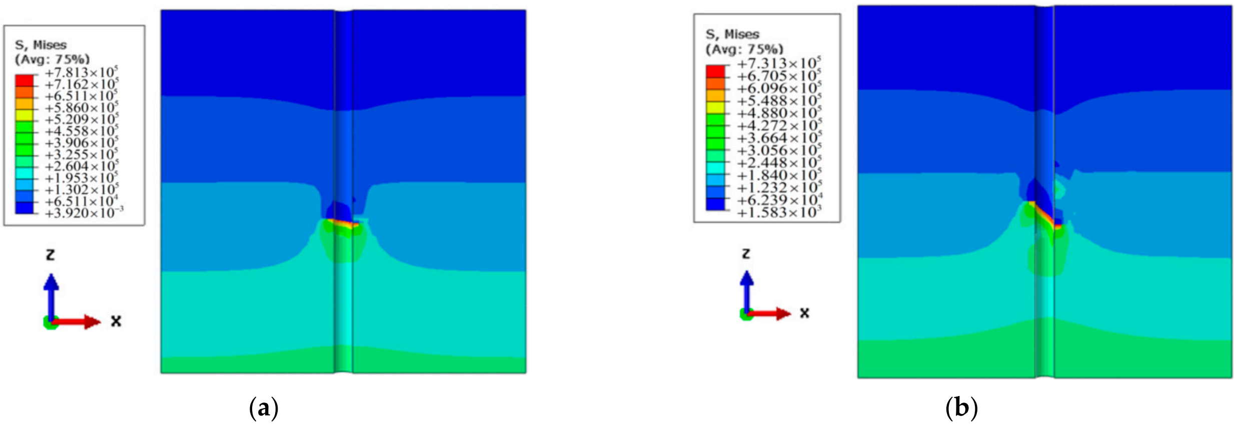

Figure 14. Von Mises stress nephograms of P1 and P2 under the same indentation displacement. (**a**) P1; (**b**) P5.

The distance from the helical pile close to the inner wall is 0.02 m, i.e., 0.004 D, and the displacement and stress values outside the pile along the depth direction are shown in Figure 15. The displacement first increases, then decreases along the depth direction, and tends to zero at infinite depth. The peak displacement depth appears at the top of the helical blade; thus, the larger the pitch, the higher the peak value. The peak displacement is about 0.1 m. The displacement drops sharply in the five curves at a depth of 25 m. The stress–depth curve reaches a second peak at the top and a maximum at the bottom of the blade. The first peak value is about 0.6 MPa and the second peak value is about 0.5 MPa.

Further calculations were performed with pitch p = 1.5, 6, and 10 m, and compared with the above results. As shown in Figure 16a,b, the bearing capacity of P10 is much lower than those of other conditions, and the compressive bearing capacity of P6 is also smaller, whereas the compressive stress gradually decreases. Therefore, the increase in bearing capacity is limited, and the bearing capacity will begin to decrease when the pitch reaches a certain value.

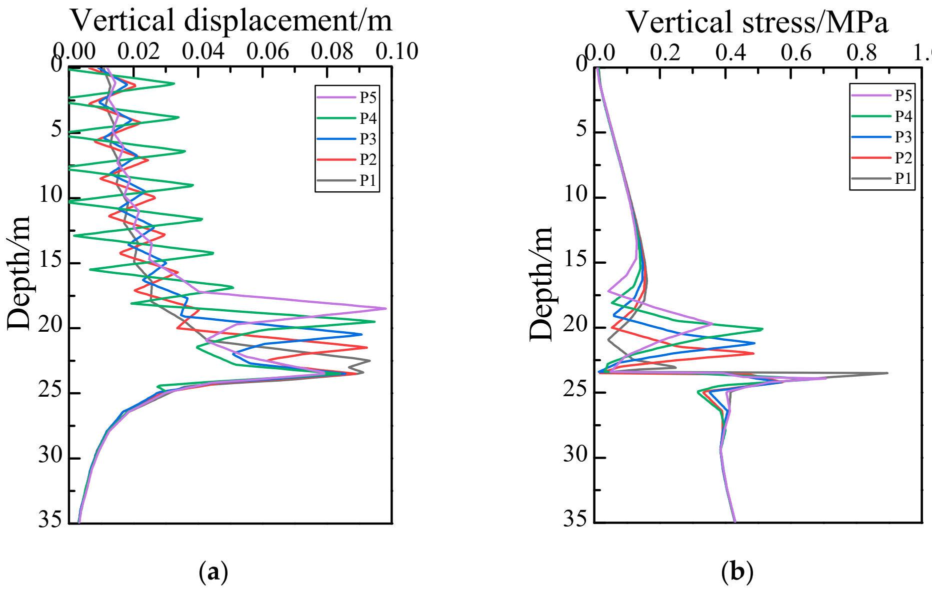

Figure 15. Variation of displacement and stress with depth. (**a**) Indentation displacement–depth curves; (**b**) Stress–depth curves.

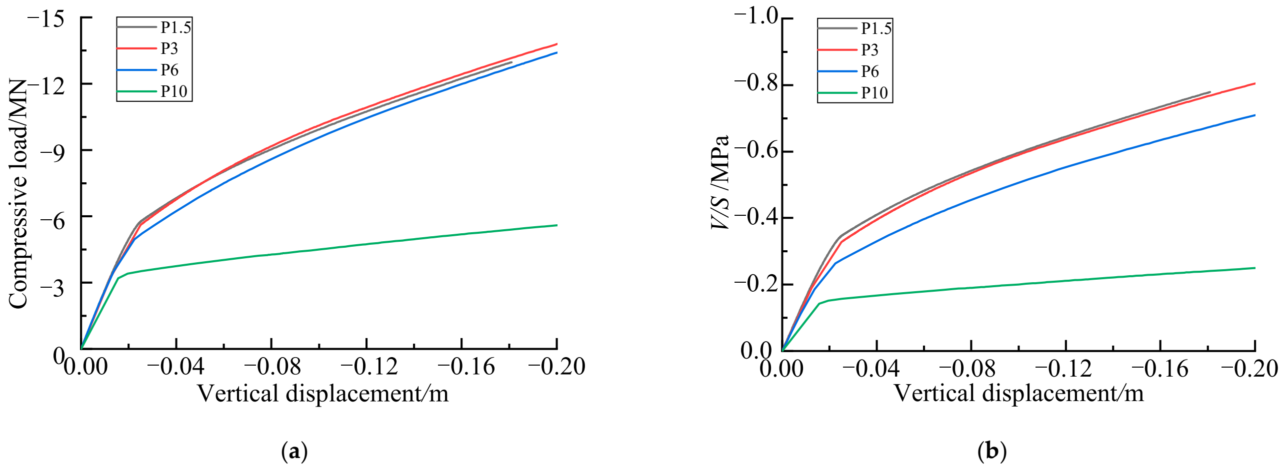

Figure 16. Compression bearing characteristics curves. (**a**) Load-displacement curves; (**b**) V/S-displacement curves.

4.3. Tensile Capacity

Uplift load-displacement curves of helical piles with different pitches after excessive uplift displacement were obtained, as shown in Figure 17a. The pull-out load increases with increasing pull-out displacement, and no obvious inflection point is observed on the curves. Under the same displacement, P4 and P5 result in higher uplift capacities. When the pullout displacement is 0.1 M, the P1 value is 8.13 Mn and the P4 value is 8.88 MN, representing an increase of 9.23%.

To eliminate the influence of steel consumption, the ratio of bearing capacity, V, to blade area, S, was studied. As shown in Figure 17b, P2 and P3 result in a larger pull-out force per unit area at the same displacement, while those of P1 and P5 are smaller. When the displacement of the pile top is 0.1 m, the pull-out force per unit area of the helical pile with each pitch is about 0.5 MPa. Combined with uplift and compression, P2 offers the best bearing capacity, with a larger bearing capacity per unit area. Therefore, the increase in pitch has a limited effect on bearing capacity. If a certain limit is exceeded, the increase in pitch will reduce the bearing capacity of the structure.

The displacement and stress under each working condition were extracted along the depth direction outside the pile at 0.02 m away from the pile, as shown in Figure 18.

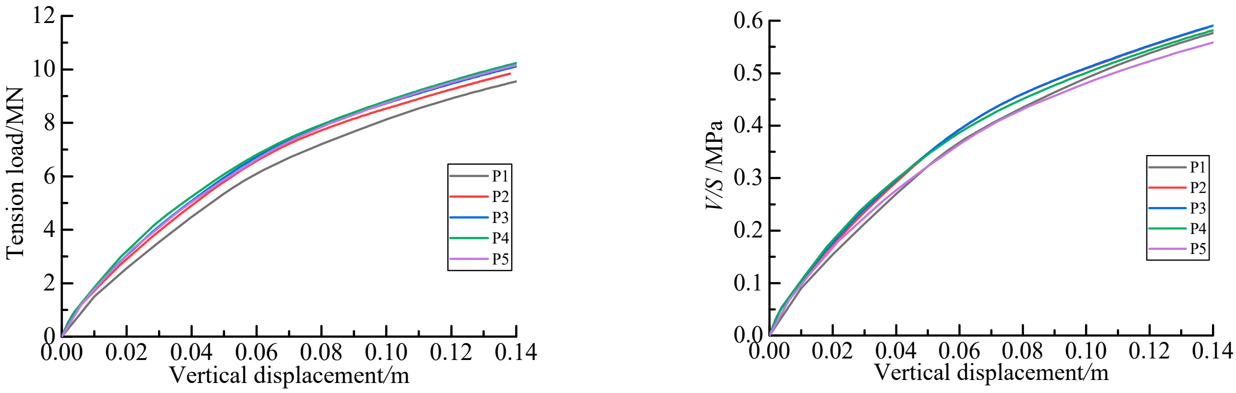

(**a**) (**b**)

Figure 17. Uplift bearing characteristics of helical pile with different pitches. (**a**) Load-displacement curves; (**b**) V/S-displacement curves.

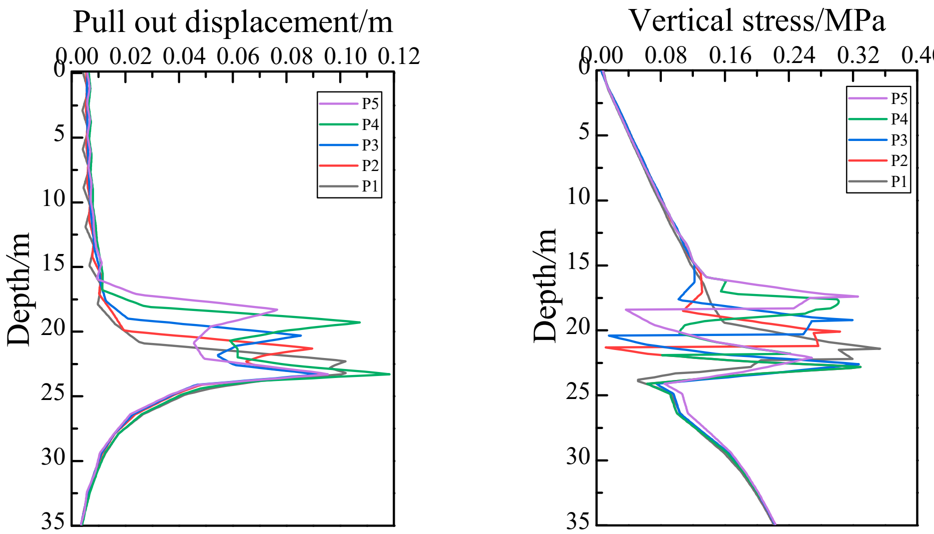

(**a**) (**b**)

Figure 18. Displacement and stress distribution of soil outside pile along the depth direction. (**a**) P2; (**b**) P3.

The displacement and stress first increase then decrease, and the main changes are concentrated in the position of the spiral blade. The two peaks in the figure appear at the two ends of the spiral blade. Therefore, the larger the screw pitch, the larger the helical pile disturbance to the soil.

Further results were obtained for pitch p = 1.5 m, 6 m, and 10 m. As shown in Figure 19a,b, the uplift bearing capacities in the front section with P6 and P10 are slightly larger than those with P1.5 and P3; however, the uplift bearing capacities of P10 after a displacement of 0.04 m and P6 after a displacement of 0.08 m are smaller than those of P1.5 and P3, and that of P10 decreases greatly. The pull-out stresses of P1.5 and P3 are consistent, whereas those of P6 and P10 are much smaller.

When the displacement reaches 0.1 m, V/S values were obtained for each condition. As shown in Figure 20, V/S first increases then decreases with pitch, the compressive stress reaches a peak value at a pitch of 2 m, and the tensile stress reaches a maximum value at a pitch of 3 m. Therefore, in order to reduce costs, the pitch should not be too large.

The comprehensive compressive bearing capacity and uplift bearing capacity of the P2 condition result in a higher bearing capacity per unit blade area. That is, when the pitch is 0.4 times the blade diameter, the helical pile balances both the economic and bearing capacity factors. Therefore, the helical pile with 0.4D was selected for further analysis.

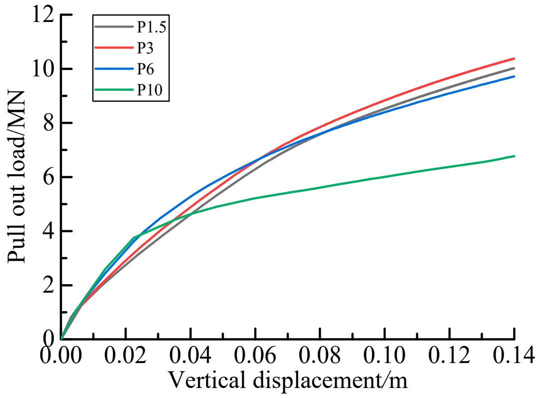

(**a**)

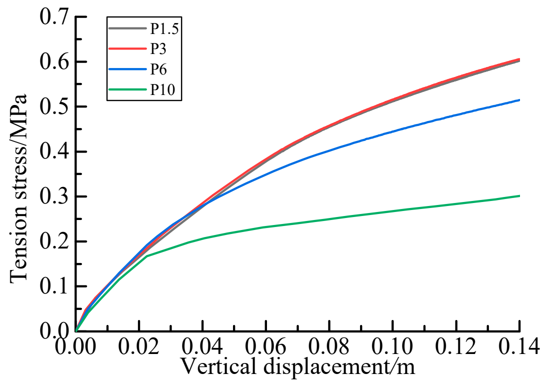

(**b**)

Figure 19. Uplift bearing characteristics of helical pile. (**a**) Load-displacement curves; (**b**) V/S-displacement curves.

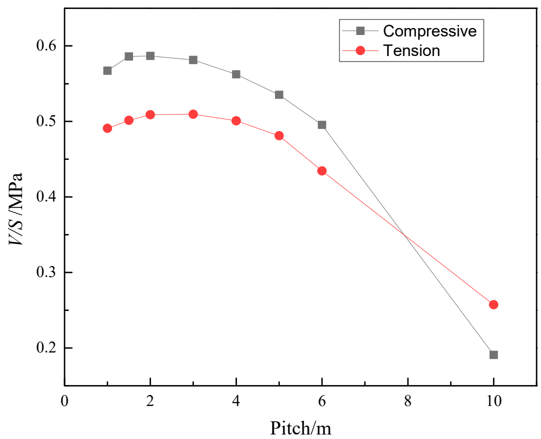

Figure 20. V/S ratio of helical pile with different pitches at displacement of 0.1 m.

5. Effect of Blade Diameter on Bearing Capacity of Single Helical Pile

5.1. Calculation Conditions

To explore the influence of helical blade diameter on the bearing characteristics of the helical pile, blade diameters D = 3 m, 4 m, 5 m, 6 m, and 7 m, i.e., D/d = 1.5, 2, 2.5, 3, and 3.5, were considered. The specific pile parameters are listed in Table 4.

Table 4. Helical pile parameters for various spiral blade diameters.

Items	D3	D4	D5	D6	D7
Pile diameter (m)	2	2	2	2	2
Number of blades	1	1	1	1	1
Blade depth (m)	25	25	25	25	25
Blade diameter (m)	3	4	5	6	7
Pitch (m)	2	2	2	2	2
Distance between blade and pile bottom (m)	1.5	1.5	1.5	1.5	1.5

5.2. Compressive Capacity

The compressive load-displacement curves of helical piles with different spiral blade diameters after applying excessive vertical downward displacement were obtained, as shown in Figure 21. The curves can be divided into two sections, and the trends of the curves in the first section were consistent under the five conditions. In the second section, the bearing capacity of conditions D3, D4, and D5 increase, in turn, with decreasing slope, with small differences among conditions D5, D6, and D7. When the displacement is 0.3 m, The compressive capacity of D3 is 13.75 MN and D6 is 17.14 MN, resulting in an increase in compressive bearing capacity of 24.65%.

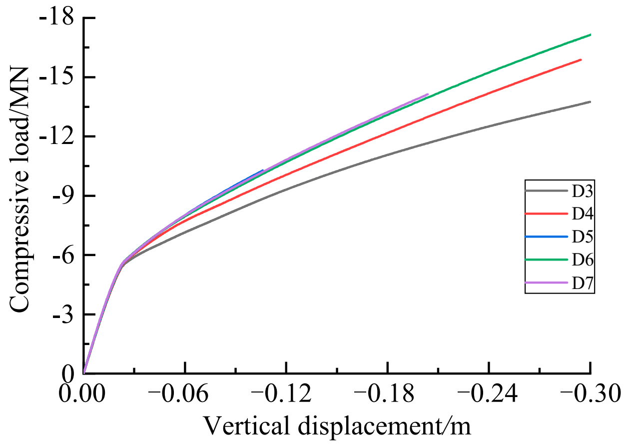

Figure 21. Compressive load-displacement curves of helical pile with various diameters.

When a bearing load of 9 MN is applied, the displacements are 0.1108 m, 0.0786 m, and 0.0797 m under conditions D3, D5, and D7, respectively.

The region most prone to damage is the connection between the helical blade and the straight rod. Displacements of the soil under conditions D3, D4, and D5 were extracted and compared. The depth was 25.02 m and the radial distance from the center was 1.02 m. The displacement of soil around the pile under the same pile top displacement of 0.1 m and the same load of 9 MN is taken, as shown in Figure 22. The position of the helical blade has a greater impact on soil displacement. Soil disturbance caused by the lower edge of the blade on the soil can be observed. When the displacement of the same pile top is 0.1 m, the soil displacement for D3 and D4 are similar and larger than that of D5. When the load is 9 MN, the displacements of D3, D4, and D5 decrease, in turn, and the circumferential circle decreases gradually. Therefore, the larger the diameter, the smaller the load per unit soil, and D5 exhibits the best bearing characteristics.

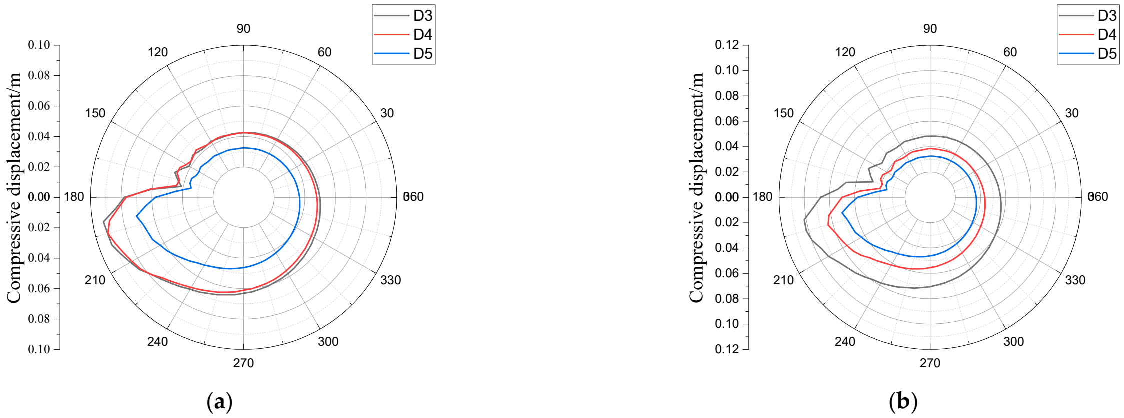

Figure 22. Distribution of soil displacement outside pile under compression and bearing load. (**a**) Displacement under compression of 0.1 m; (**b**) 9 MN compressive load.

5.3. Tensile Capacity

The pull-out load-displacement curves of helical piles with different helical blades were obtained after applying excessive vertical upward displacement, as shown in Figure 23. There is no obvious inflection point in the pull-out load-displacement curves, and the bearing load is similar for each working condition. The curves for D5, D6, and D7 almost coincide, and no obvious differences can be observed. However, the bearing capacities increase gradually with D3, D4, and D5, suggesting that the uplift bearing capacity increases with increasing blade diameter.

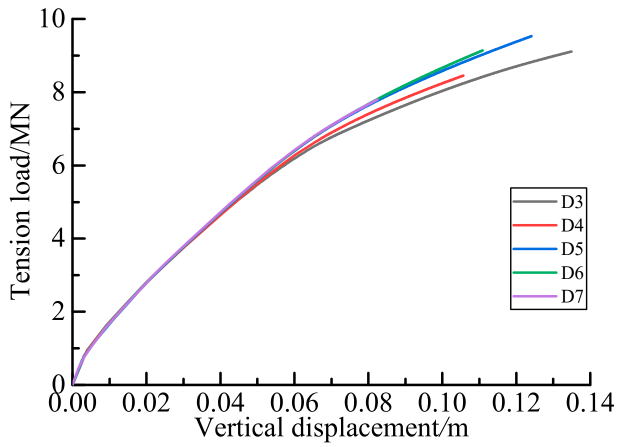

Figure 23. Uplift load-displacement curves of screw piles with various blade diameters.

When the displacement is 0.12 m, the uplift load is 8.70 MN and 9.38 MN for D3 and D5, respectively, representing an increase in uplift capacity of 7.82%.

6. Study on Bearing Capacity of Multi-Blade Helical Pile

6.1. Calculation Conditions

The influence of various conditions, such as blade diameter, blade spacing, and number of blades, on the vertical bearing capacity were analyzed. Diameter D = 3 m, 4 m, and 5 m, i.e., D/d = 1.5, 2 and 2.5, and various spacing and multiple blades were studied. Specific parameter values for each working condition are listed in Table 5.

Table 5. Multi-blade finite element model.

Condition	Number of Blades	Diameter (m)	Blade Spacing (m)
N1-D3	1	3	0
N1-D4	1	4	0
N1-D5	1	5	0
N2-D3-L3	2	3	3
N2-D3-L5	2	3	5
N2-D3-L8	2	3	8
N2-D4-L3	2	4	3
N2-D4-L5	2	4	5
N2-D4-L8	2	4	8
N2-D4-L12	2	4	12
N2-D5-L3	2	5	3
N2-D5-L5	2	5	5
N2-D5-L8	2	5	8
N3-D5-L3	3	5	3
N3-D5-L5	3	5	5
N4-D5-L3	4	5	3
N5-D5-L3	5	5	3

6.2. Bearing Capacity of Two-Blade Helical Pile

6.2.1. Compressive Capacity

Regarding the study of blade spacing in Section 5.1, the compressive load-displacement curve obtained using the finite element method is shown in Figure 24. The compression efficiency coefficient of the multi-blade spiral pile is introduced here as η_c, which can be calculated as:

$$\eta_c = \frac{Q_c}{n \cdot Q_{cs}} \tag{2}$$

where Q_c is the ultimate compressive bearing capacity of the multi-blade spiral pile, Q_{cs} is the ultimate compressive bearing capacity of the single-blade spiral pile, and n is the number of spiral blades.

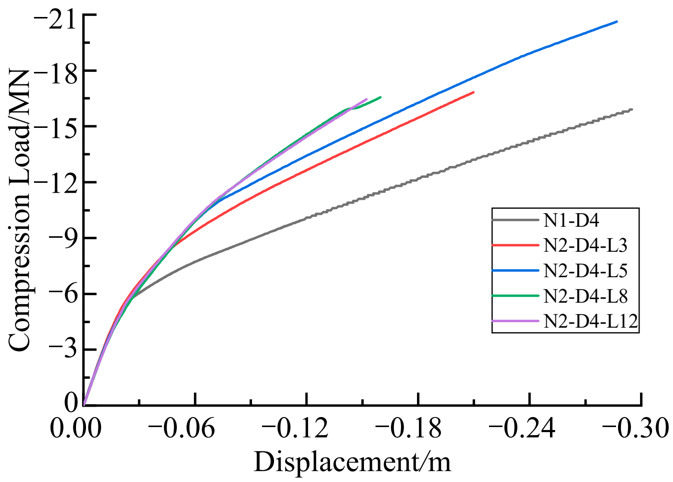

Figure 24. Compressive load-displacement curves (D/d = 2, n = 2).

The ultimate bearing capacity under a compressive displacement of 0.1 m was extracted under each working condition, and the compression efficiency coefficient was calculated, as shown in Table 6. The compression efficiency gradually increases with blade spacing from 0.75D to 2D; however, the change is small when the blade spacing is greater than 2D, indicating that critical spacing, in terms of ultimate compression bearing capacity, is reached at around 2D. Further increasing the spacing will have no positive effect on the increase in bearing capacity. Thus, to improve the overall bearing capacity, another method must be used. The bearing capacity of the double-blade screw pile with a spacing of 1.25D is 6.40% higher compared with a spacing of 0.75D, and 12.19% higher than with a spacing of 2D.

Table 6. Compression efficiency coefficient (D/d = 2, n = 2).

Conditions	Compressive Bearing Capacity (MN)	Compression Efficiency Coefficient
N1-D4	9.2997	—
N2-D4-L3	11.6647	0.6272
N2-D4-L5	12.4115	0.6673
N2-D4-L8	13.1939	0.7094
N2-D4-L12	13.0872	0.7036

To study the relationship between compression efficiency coefficient and blade spacing, i.e., l/D, the compressive load-displacement curves were obtained for various blade diameters by comparing the conditions D = 3 m and D = 5 m in Section 6.1, as shown in Figure 25. The ultimate bearing capacity was extracted, and the compression efficiency coefficient was calculated, as shown in Table 7.

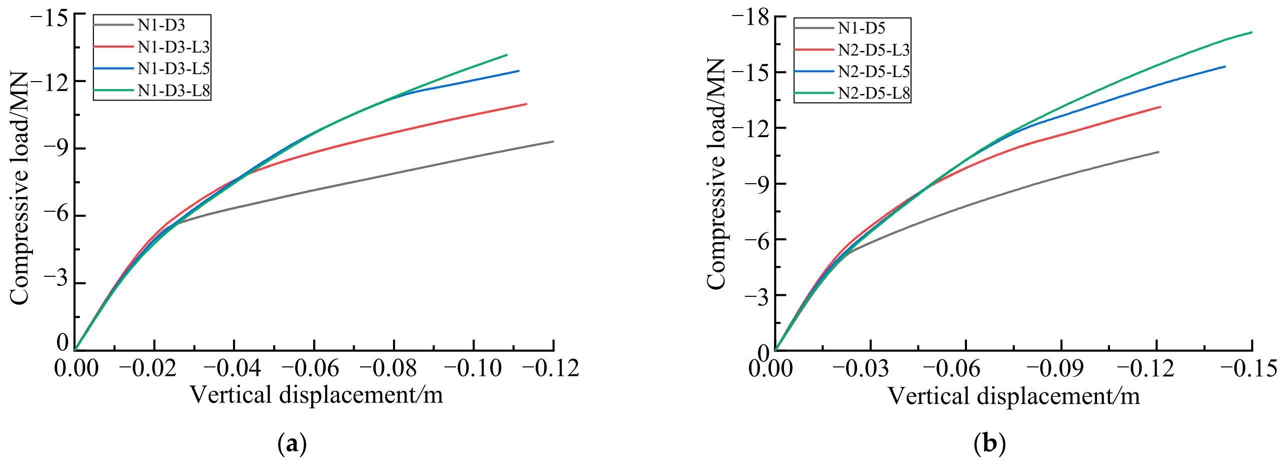

Figure 25. Compressive load-displacement curves with various blade spacing l/D. (**a**) D/d = 1.5, n = 2; (**b**) D/d = 2.5, n = 2.

Table 7. Compression efficiency coefficient with various blade spacing l/D.

Condition	Compressive Bearing Capacity (MN)	Compression Efficiency Coefficient	l/D
N1-D3	8.6113	—	—
N2-D3-L3	10.5038	0.6099	1.00
N2-D3-L5	12.0406	0.6991	1.67
N2-D3-L8	12.6503	0.7345	2.67
N1-D5	9.8307	—	—
N2-D5-L3	12.1016	0.6155	0.60
N2-D5-L5	13.1990	0.6713	1.00
N2-D5-L8	13.9001	0.7070	1.60

The correlation between the compression efficiency coefficient and the blade spacing was obtained by comparing the conditions in Section 5.1. The fitted curve is shown in Figure 26. The overall correlation is good. The fitting formula, which can only be applied in the case of small spacing, is:

$$\eta_c = 0.6503 \cdot \left(\frac{l}{D}\right)^{0.1299} \tag{3}$$

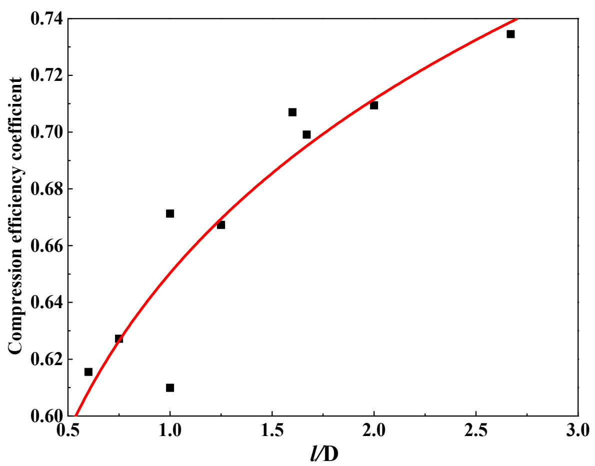

Figure 26. Correlation between compression efficiency coefficient and blade spacing.

6.2.2. Tensile Capacity

The curve of uplift load displacement was obtained by applying excessive vertical uplift displacement, as shown in Figure 27. The curves for helical blade spacing greater than 5 m almost coincide, indicating that the critical adjacent blade spacing is reached at 1.25D. The uplift efficiency coefficient of the multi-blade helical pile, η_u, can be introduced and calculated as:

$$\eta_u = \frac{Q_u}{n \cdot Q_{us}} \tag{4}$$

where Q_u is the ultimate uplift bearing capacity of the multi-blade helical pile, Q_{us} is the ultimate uplift bearing capacity of the single-blade helical pile, and N is the number of helical blades.

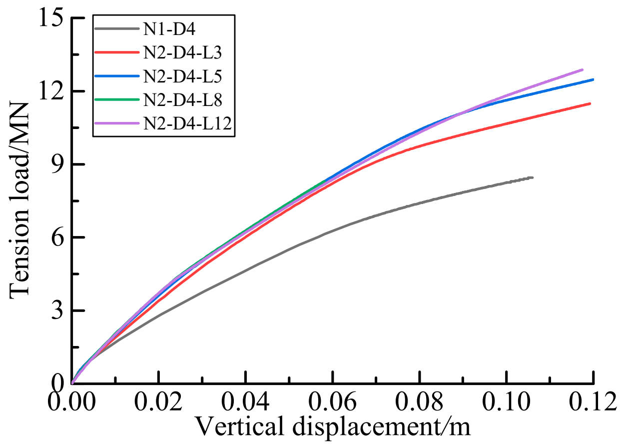

Figure 27. Uplift load-displacement curves (D/d = 2, n = 2).

The ultimate uplift bearing capacity at 0.1 m uplift displacement under the comparison condition was extracted and the uplift efficiency coefficient was calculated, as shown in Table 8. When the blade spacing is more than 5 m, the pullout efficiency coefficient is between 0.62 and 0.63, which is 9.06–10.98% higher than with a blade spacing of 3 m. The drawing efficiency coefficient is clearly less than the compression efficiency coefficient, which indicates that increasing blade spacing is more helpful in improving the compressive bearing capacity, and the uplift bearing capacity is improved slightly. This is because the soil between the two blades forms a cylindrical block, which significantly improves the compressive bearing capacity. In the case of drawing, the soil cylinder on the blade is the main resistance, and the soil cylinder on the upper part of the multi-blade is more consistent with that of the single blade. That is, the soil cylinder on the blade changes with the increasing number of blades. The extra bearing capacity may be due to expansion of the failure surface beyond the range of the blade diameter, as described by other failure modes.

Table 8. Uplift efficiency coefficient (D/d = 2, n = 2).

Condition	Uplift Bearing Capacity (MN)	Uplift Efficiency Coefficient
N1-D4	8.2430	—
N2-D4-L3	10.6562	0.5729
N2-D4-L5	11.6215	0.6248
N2-D4-L8	11.7104	0.6296
N2-D4-L12	11.8247	0.6358

To study the relationship between the uplift efficiency coefficient and blade spacing, i.e., l/D, uplift load-displacement curves were obtained using conditions N1 and N3 in Section 5.1 and by varying the blade diameter, as shown in Figure 28. The ultimate uplift capacity was extracted, and the uplift efficiency coefficient was calculated, as presented in Table 9.

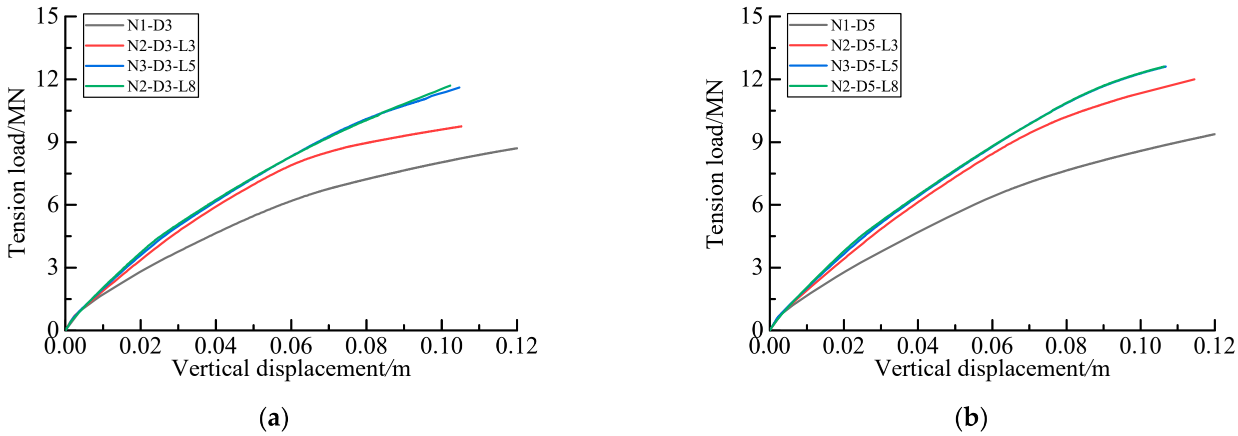

Figure 28. Uplift load-displacement curves for various blade spacing l/D. (**a**) D/d = 1.5, n = 2; (**b**) D/d = 2.5, n = 2.

Table 9. Uplift efficiency coefficient for various blade spacing l/D.

Condition	Uplift Bearing Capacity (MN)	Uplift Efficiency Coefficient	l/D
N1-D3	8.0271	—	—
N2-D3-L3	9.5893	0.5568	1.00
N2-D3-L5	11.3548	0.6593	1.67
N2-D3-L8	11.5326	0.6696	2.67
N1-D5	8.5732	—	—
N2-D5-L3	11.3421	0.5769	0.60
N2-D5-L5	12.2693	0.6240	1.00
N2-D5-L8	12.3201	0.6266	1.60

Correlation between the compression efficiency coefficient and blade spacing was obtained by comparing the conditions in Section 5.1. The fitted curve is shown in Figure 29. The fitting formula, which is only applicable in the case of small spacing, is:

$$\eta_u = 0.5998 \cdot \left(\frac{l}{D}\right)^{0.1110} \quad (5)$$

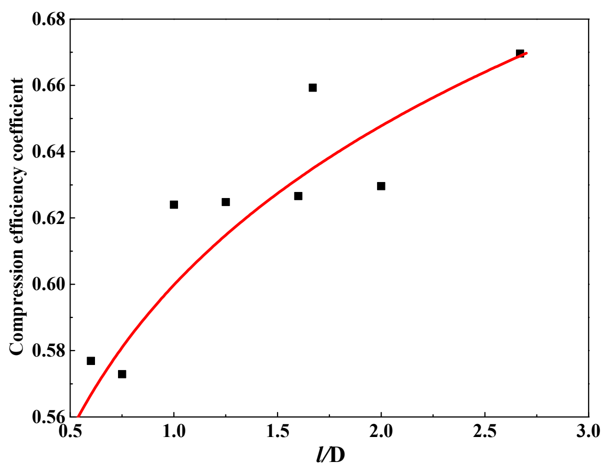

Figure 29. Relationship between pullout efficiency coefficient and blade spacing.

A worse degree of fit was obtained with the uplift formula compared with the compression formula, and the coefficient value in the formula was also slightly smaller, which is related to differences in the failure modes due to soil compression and uplift.

6.3. Bearing Capacity of Multi-Blade Helical Pile

6.3.1. Compressive Capacity

To compare the effects of different blade numbers in Section 5.1, the load-displacement curves were obtained after applying excessive downforce displacement, as shown in Figure 30. As the number of blades increases, the bearing capacity also gradually improves. To consider the economic benefits of the foundation bearing capacity, the ultimate bearing capacity at a downforce displacement of 0.1 m was extracted and the downforce efficiency coefficient was calculated, as shown in Table 10.

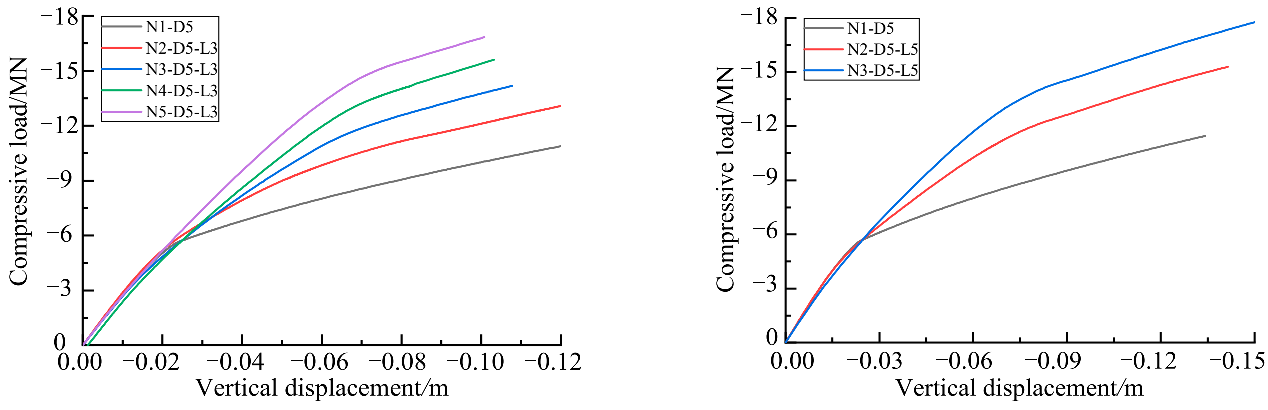

Figure 30. Compressive load-displacement curves of multi-blade helical pile. (**a**) $D/d = 2$, $l/D = 0.6$, $n = 1$–5; (**b**) $D/d = 2$, $l/D = 1$, $n = 1$–3.

Table 10. Compression efficiency coefficient of multi-blade helical pile.

Conditions	Compressive Bearing Capacity (MN)	Compression Efficiency Coefficient
N1-D5	9.8307	—
N2-D5-L3	12.1016	0.6155
N3-D5-L3	13.7629	0.4667
N4-D5-L3	15.3937	0.3915
N5-D5-L3	16.7807	0.3414
N2-D5-L5	13.1990	0.6713
N3-D5-L5	15.1041	0.5121

From Table 10, it can be seen that, as the number of blades increases, the compression efficiency coefficient decreases; that is, increasing the number of blades also increases the amount of steel required. Therefore, material is wasted to a certain extent because the compressive bearing capacity does not significantly increase.

6.3.2. Tensile Capacity

To compare the effects of different blade numbers in Section 5.1, load-displacement curves after applying excessive uplift displacement were obtained, as shown in Figure 31. The foundation bearing capacity increases with the increasing number of blades; however, the growth in bearing capacity slows down considerably with five and six blades, and the effect is no longer significant. The uplift efficiency coefficient was calculated, as shown in Table 11.

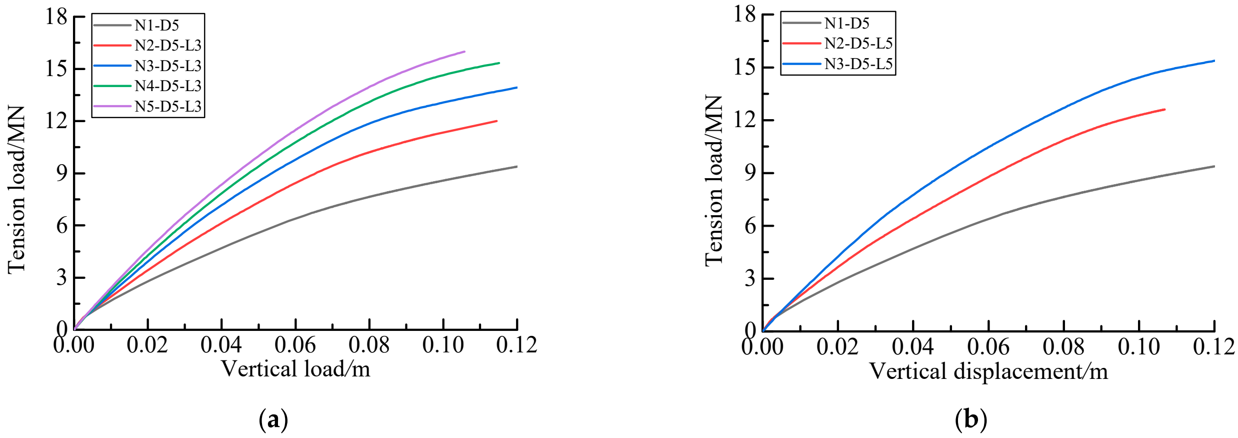

Figure 31. Uplift load-displacement curves of multi-blade helical pile. (**a**) $D/d = 2$, $l/D = 0.6$, $n = 1$–5; (**b**) $D/d = 2$, $l/D = 1$, $n = 1$–3.

Table 11. Uplift efficiency coefficient of multi-blade helical pile.

Condition	Uplift Bearing Capacity (MN)	Uplift Efficiency Coefficient
N1-D5	8.5732	—
N2-D5-L3	11.3421	0.6615
N3-D5-L3	13.0618	0.5079
N4-D5-L3	14.6317	0.4267
N5-D5-L3	15.6681	0.3655
N2-D5-L5	12.2693	0.7156
N3-D5-L5	14.4335	0.5612

From Table 11, it can be seen that the pullout efficiency coefficient decreases with the increasing number of blades. The pullout capacity with five blades is only 38.14% higher than with two blades; however, much more steel is required for five blades. Therefore, selecting two blades will have a positive effect on improving the bearing capacity while minimizing the cost.

7. Conclusions

This paper analyzed the bearing characteristics of a helical pile and an ordinary pile without blades. The advantages of the helical pile in resisting vertical load were highlighted. When the single-blade helical pile is long and the blade is deep, the horizontal load-displacement curves and moment rotation curves of the single-blade helical pile and ordinary pile are almost coincident. Under vertical compression, the bearing capacity of the helical pile increases by 149% compared with the ordinary pile. With vertical drawing, the bearing capacity increases 1.49-fold.

The results show that the highest bearing capacity per unit area is obtained when pitch $p = 2$ m and $p = 3$ m, that is, 0.08 or 0.12 times the pile length. If the pitch is too large, installing and constructing the pile is inconvenient. Moreover, the bearing capacity will be greatly reduced.

Blade diameter has a large influence on vertical bearing capacity. When the diameter is too large, material resources are wasted and the bearing capacity is not significantly improved. Through calculations, it was found that when the diameter of the helical blade is 2.5D, the bearing capacity is higher and the compression and pullout characteristics are fully utilized.

In general, the higher the number of blades, the higher the bearing capacity of the foundation; however, the efficiency of the helical blades is closely related to the spacing. The results show that the critical value of double-helical blade foundation capacity in single-layer sand is reached when the blade spacing $L = 2D$, and further increasing L has little effect on bearing capacity. As the number of blades increases, the bearing capacity of the multi-blade helical pile foundation gradually increases; however, the efficiency gradually decreases. It is recommended that the number of blades should not exceed three, to ensure the bearing efficiency remains high. The results provide a reference for further analysis of pile group foundations.

It should be noted that the paper does not take into account the effect of cyclic loading, which involves issues such as stiffness problems and cumulative deformation, which could be the subject of subsequent research. There is also a lack of research on the foundation load bearing characteristics under different soil properties, which will also be included as a subsequent study.

Author Contributions: Conceptualization, Y.L., J.X., C.L., P.Z. and H.D.; software, Q.C., P.Z, C.L. and J.X.; validation, Y.L. and H.D.; writing—original draft preparation, Y.L., J.X., C.L., P.Z., Q.C. and H.D.; writing—review and editing, J.X., C.L. and Q.C.; supervision, Y.L. and H.D. All authors have read and agreed to the published version of the manuscript.

Funding: This research received no external funding.

Institutional Review Board Statement: Not applicable.

Informed Consent Statement: Not applicable.

Data Availability Statement: Not applicable.

Conflicts of Interest: The authors declare no conflict of interest.

References

1. Mitchell, A. On Submarine Foundations; Particularly the Screw Pile and Moorings. *Min. Proc. Inst. Civ. Eng.* **1848**, *7*, 108–132. [CrossRef]
2. Lutenegger, A.J. Historical Development of Iron Screw-Pile Foundations: 1836–1900. *Int. J. Hist. Eng. Technol.* **2013**, *81*, 108–128. [CrossRef]
3. Li, J.; Wang, G.; Li, Z.; Yang, S.; Chong, W.T.; Xiang, X. A review on development of offshore wind energy conversion system. *Int. J. Energy Res.* **2020**, *44*, 9283–9297. [CrossRef]
4. Soares-Ramos, E.P.; de Oliveira-Assis, L.; Sarrias-Mena, R.; Fernández-Ramírez, L.M. Current status and future trends of offshore wind power in Europe—ScienceDirect. *Energy* **2020**, *202*, 117787. [CrossRef]
5. Wei, Y.; Zou, Q.P.; Lin, X. Evolution of price policy for offshore wind energy in China: Trilemma of capacity, price and subsidy. *Renew. Sustain. Energy Rev.* **2021**, *136*, 110366. [CrossRef]
6. Zhang, S.; Wei, J.; Chen, X.; Zhao, Y. China in global wind power development: Role, status and impact. *Renew. Sustain. Energy Rev.* **2020**, *127*, 109881. [CrossRef]
7. Ren, Y.; Vengatesan, V.; Shi, W. Dynamic Analysis of a Multi-column TLP Floating Offshore Wind Turbine with Tendon Failure Scenarios. *Ocean Eng.* **2022**, *245*, 110472. [CrossRef]
8. Wang, Y.; Shi, W.; Michailides, C.; Wan, L.; Kim, H.; Li, X. WEC shape effect on the motion response and power performance of a combined wind-wave energy converter. *Ocean Eng.* **2022**, *250*, 111038. [CrossRef]
9. Isorna, R.; Blanc, M.; Thorel, L.; Kotronis, P.; Dano, C.; Philippe, M. Axial behaviour of jacket piles for offshore wind turbines. *Int. J. Phys. Model. Geotech.* **2016**, *17*, 229–245. [CrossRef]
10. Kong, D.; Deng, M.; Xu, Y. Study on Calculation of Pile Sliding Interval of Large-Diameter Steel Pipe Piles on Offshore Platforms. *Math. Probl. Eng.* **2019**, *2019*, 3549296.
11. Byrne, B.W.; Houlsby, G.T. Helical piles: An innovative foundation design option for offshore wind turbines. *Philos. Trans. R. Soc.* **2015**, *373*, 20140081. [CrossRef] [PubMed]
12. Zaaijer, M.B. Foundation modelling to assess dynamic behaviour of offshore wind turbines. *Appl. Ocean Res.* **2006**, *28*, 45–57. [CrossRef]
13. Jonkman, J.; Musial, W. *Offshore Code Comparison Collaboration (OC3) for IEA Task 23 Offshore Wind Technology and Deployment*; Technical Report No. NREL/TP-5000-48191; National Renewable Energy Laboratory: Golden, CO, USA, 2010.
14. Rendon, E.A.; Manuel, L. Long-term loads for a monopile-supported offshore wind turbine. *Wind Energy* **2012**, *17*, 209–223. [CrossRef]
15. Carswell, W.; Arwade, S.R.; DeGroot, D.J.; Lackner, M.A. Soil–structure reliability of offshore wind turbine monopile foundations. *Wind Energy* **2015**, *18*, 483–498. [CrossRef]
16. Alati, N.; Failla, G.; Arena, F. Seismic analysis of offshore wind turbines on bottom-fixed support structures. *Philos. Trans. R. Soc.* **2015**, *373*, 20140086. [CrossRef]

17. Balla, A. The resistance to breaking out of mushroom foundations for pylons. In Proceedings of the Fifth International Conference on Soil Mechanics and Foundation Engineering, Paris, France, 17–22 July 1961.
18. Majer, J. Zur berechnung von zugfundamenten. *Osterreichische Bauz.* **1955**, *10*, 85–90.
19. Matsuo, M. Study on the Uplift Resistance of Footing. *Soils Found.* **1967**, *7*, 1–37. [CrossRef]
20. Meyerhof, G.G.; Adams, J.I. The ultimate uplift capacity of foundations. *Can. Geotech. J.* **2011**, *5*, 225–244. [CrossRef]
21. Mors, H. The behaviour of mast foundations subjected to tensile force. *Bautechnik* **1959**, *36*, 367–378.
22. Zhu, C.; Chu, X. Calculation of ultimate extraction resistence of anchoring plates in calcaress sands. *Rock Soil Mech.* **2003**, *24*, 153–158.
23. Mohajerani, A.; Bosnjak, D.; Bromwich, D. Analysis and design methods of screw piles: A review. *Soils Found.* **2016**, *56*, 115–128. [CrossRef]
24. Harnish, J.; Naggar, M. Large Diameter Helical Pile Capacity—Torque Correlations. *Can. Geotech. J.* **2017**, *54*, 968–986. [CrossRef]
25. Spagnoli, G.; de Hollanda Cavalcanti Tsuha, C.; Oreste, P.; Mendez Solarte, C.M. A sensitivity analysis on the parameters affecting large diameter helical pile installation torque, depth and installation power for offshore applications. *DFI J. J. Deep Found. Inst.* **2019**, *12*, 171–185. [CrossRef]
26. Polishchuk, A.I.; Maksimov, F.A. Numerical Analysis of Helical Pile–Soil Interaction under Compressive Loads. In *IOP Conference Series: Materials Science and Engineering*; IOP Publishing: Bristol, UK, 2017; Volume 262, p. 012099.
27. Abbase, H.O.; Ali, O.K. Parameters Affecting Screw Pile Capacity Embedded in Soft Clay Overlaying Dense Sandy Soil. In *IOP Conference Series: Materials Science and Engineering*; IOP Publishing: Bristol, UK, 2020; Volume 745.
28. Prasad, Y.; Rao, S.N. Lateral capacity of helical piles in clays. *J. Geotech. Eng.* **1996**, *122*, 938–941. [CrossRef]
29. Ding, H.Y.; Wang, L.; Zhang, P.Y. Study on the Lateral Bearing Capacity of Single-Helix Pile for Offshore Wind Power. In Proceedings of the ASME 2018 37th International Conference on Ocean, Offshore and Arctic Engineering OMAE2018, Madrid, Spain, 17–22 June 2018.
30. Ding, H.; Wang, L.; Zhang, P.; Liang, Y.; Tian, Y.; Qi, X. The Recycling Torque of a Single-Plate Helical Pile for Offshore Wind Turbines in Dense Sand. *Appl. Sci.* **2019**, *9*, 4105. [CrossRef]
31. Al-Baghdadi, T.A.; Brown, M.J.; Knappett, J.A.; Al-Defae, A.H. Effects of vertical loading on lateral screw pile performance. *Proc. Inst. Civ. Eng.-Geotech. Eng.* **2017**, *170*, 259–272. [CrossRef]
32. Hibbitt, Karlsson & Sorensen, Inc. *ABAQUS/Standard User's Manual*; ABAQUS; Hibbitt, Karlsson & Sorensen, Inc.: Pawtucket, RI, USA, 2010.
33. Wang, L.; Zhang, P.; Ding, H.; Tian, Y.; Qi, X. The uplift capacity of single-plate helical pile in shallow dense sand including the influence of installation. *Mar. Struct.* **2020**, *71*, 102697. [CrossRef]